scientific reports

Check for updates

OPEN

Network topology and recovery delay thresholds determine cascading failure vulnerability in sports systems

Chulwook Park[1,2,3]✉

Network topology fundamentally determines how cascading failures propagate through sports systems, yet the risk thresholds governing this relationship remain unquantified. We developed a network-agent model comparing four structural configurations through failure propagation dynamics, protection strategies, and recovery mechanisms across random, regular, small-world, and scale-free networks. Scale-free structures, characteristic of star-player dependent teams, exhibit 57% higher vulnerability than regular counterparts, with a Network Vulnerability Index of 1.24 versus 0.79. Immediate recovery interventions ($r_t = 1$) effectively prevent cascading failures, while delayed responses ($r_t \geq 2$) trigger exponential propagation. Phase space analysis reveals distinct stability basins, with scale-free configurations occupying the largest failure-dominant region at 43% of the phase space. Empirical validation against professional injury cascade records and international league shutdown data confirms strong agreement between model predictions and observed outcomes, with leagues implementing immediate interventions recovering 26.9% faster. These findings establish quantitative thresholds for topology-aware management strategies to mitigate cascading failures in professional sports.

Keywords Network topology, Cascading failures, Agent-based modeling, Risk propagation, Recovery delay, Sports systems

Risk is an unstable characteristic that occurs between interconnected components and implies that a certain factor can seriously impact the functioning of a system[1]. In particular, a very small bias, event, or failure is thought to be a cause of a large disaster that propagates through cascading ripple effects to other parts. This is also referred to as 'network risk' because it originates from close links between nodes[2]. In fact, such risks exhibit highly diverse and complex propagation patterns[3], and researchers in various fields are attempting to understand the mechanism. They propose empirical observations, often through simulation, to investigate factors that can disturb system stability or lead to system breakdown, based on properties originating from the components, such as the structure of interpersonal connections, propagation of risks, and flow of protection[4].

In this context, network-agent algorithms have been introduced in sports science[5], with practical applications including systems dynamics modeling of sports industry risks[6] and agent-based simulations for response strategies[7]. These approaches have been applied across neuromuscular coordination[8], performance transfer dynamics[9], and match outcome prediction[10,11]. In sports networks, close interactions among individuals play a critical role in athletic ability and occupational outcomes[12], where functional variables such as neuromuscular connections lose structural stability if any component is disturbed[13,14]. While this physiological example illustrates the general principle of cascading disruption, the present study addresses risk propagation at the team and organizational level, where failure spreads through social, tactical, and institutional linkages. At this system level, emotional contagion between team members[15,16], performance streakiness[17], and injury clustering[18] all demonstrate that small disturbances can propagate through interconnected sports systems[19]. Estimating the propagation of such risks remains a central challenge, both for understanding network structures[12] and for assessing systemic risk[2]. Previous studies on network robustness have established that scale-free networks are particularly vulnerable to targeted attacks on hub nodes, while random networks are more susceptible to

[1]Department of Physical Education, Seoul National University, Seoul 08826, South Korea. [2]Systemic Risk and Resilience, International Institute for Applied Systems Analysis (IIASA), A-2361 Laxenburg, Austria. [3]Complexity Science and Evolution, Okinawa Institute of Science and Technology (OIST), Okinawa, Japan. ✉email: pcw8531@snu.ac.kr

random failures[20]. More recent work has examined how mobile agents form consensus across heterogeneous network environments through co-evolutionary dynamics[21]. However, these studies primarily addressed static node removal or uniform interaction rules without considering how the timing of recovery interventions alters propagation outcomes. The present study extends this body of work by introducing recovery delay as a dynamic parameter that creates a phase transition between system resilience and cascading failure. Unlike static attack models where removed nodes remain permanently inactive, our agents actively invest in protection, imitate successful strategies, and explore alternatives, producing qualitatively different dynamics than passive node removal alone.

Risk propagation in sports contexts follows similar dynamics to those observed in system-wide crises such as the COVID-19 pandemic[22,23], where new cases can exhibit exponential growth over short time frames[24] unless immediate interventions such as social distancing and isolation are implemented[25,26]. Analogous patterns have been documented in the spread of performance-enhancing drug use across professional sports, where the absence of preventive measures allowed risk to propagate along an exponential trajectory, eroding institutional integrity and diminishing public trust[27–29]. These complex dynamics observed in sports environments can be quantitatively mapped to specific model parameters (Table 1), enabling direct comparison between simulated cascade dynamics and observed failure patterns in professional sports contexts.

Within the sports industry, issues related to delays, such as the management of off-field matters, injury treatment, player substitutions, and game scheduling, are reported as critical performance variables (referred to as 'streakiness' in sports). Yet, the model that interconnects these dynamics of individuals (represented as nodes) and the concept of intervention[30] is not widely utilized in sports systems[31]. In the context of general situational risks, 'recovery' is often viewed as a debt or immunity that must be regained. Specifically, in sports interventions, the 'recovery delay' effect is typically considered only in the context of treatment and rehabilitation[32]. Moreover, the types and number of individuals involved in these systems often remain random or undefined, and the validation of parameters remains primarily at the level of statistical variance, resulting in significant limitations in explaining the risks and protective potential[33]. The unit of intervention delay (i.e., time delay) in such a model has not been explicitly defined or elucidated[34].

To address these challenges, this study poses three specific research questions: (1) How does network topology affect failure cascade probability in sports systems? (2) What is the critical recovery delay threshold across different network structures? (3) Can immediate intervention strategies be optimized based on network characteristics? These questions guide our investigation into the interplay between network structure, risk propagation, and intervention timing in sports contexts.

Therefore, we developed a network-agent model incorporating recovery mechanisms across four fundamental network structures (random, regular, small-world, and scale-free) (Fig. 1), with agent dynamics governed by heuristics, imitation, and exploration[35,36]. The present work offers three novel contributions that extend beyond classical network robustness findings[20,21]: (1) introduction of the Network Vulnerability Index (NVI) as a single quantitative measure for cross-topology vulnerability comparison, (2) identification of critical recovery delay thresholds that differentiate system resilience from cascading failure, and (3) dual-scale empirical validation using micro-level injury cascade data (n = 77,463 events) and macro-level COVID-19 sports shutdown data (12 international leagues). These contributions bridge theoretical network models with practical risk management applications in professional sports and other interconnected systems.

Results

Characteristics of network structures

To investigate how network topology affects failure cascade dynamics, we simulated four canonical network structures representing distinct sports organizational contexts: random networks (community sports), regular networks (structured teams), small-world networks (professional athlete social networks), and scale-free networks (star-player dependent teams). Each network consisted of agent dynamics governed by protection investment, imitation, and exploration mechanisms (see Methods and Supplementary Information Sect. 1 for detailed model specification and parameter values).

In the simulation, four network structures were parameterized using standard graph models [random = n, p; regular = n, $d\,(p)$; small-world = n, p, β; scale-free = n, m], where n is the number of individuals and the remaining parameters determine connection topology (see Methods). When connection probability was low, variances in path length and connection time increased; at high connection probability with full interconnection, these variances decreased (see Supplementary Information Sect. 2.1). Eigenvector centrality

Sports Phenomenon	Description	Model Parameter	Symbol	Value Range	References
Performance streakiness	Sequential patterns of success/failure in athletic performance	Failure propagation probability	p_l	0.1–0.3	[17]
Emotional contagion	Transfer of mood and emotion between team members	Imitation probability	p_r	0.9	[15]
Attribution patterns	Cognitive processing of success and failure outcomes	Recovery delay time	r_t	1–2	[53]
Injury clustering	Temporal and spatial concentration of injuries within teams	Risk origination probability	p_n	0.1	[18]

Table 1. Mapping of observed sports phenomena to network-agent model parameters. Parameter values were calibrated based on empirical observations from sports psychology and epidemiology literature. The value ranges represent typical conditions observed in professional sports environments, where p_l captures the contagious nature of performance variations, p_r reflects the high social influence in team settings, r_t represents intervention timing in time steps, and p_n indicates baseline risk levels in athletic populations.

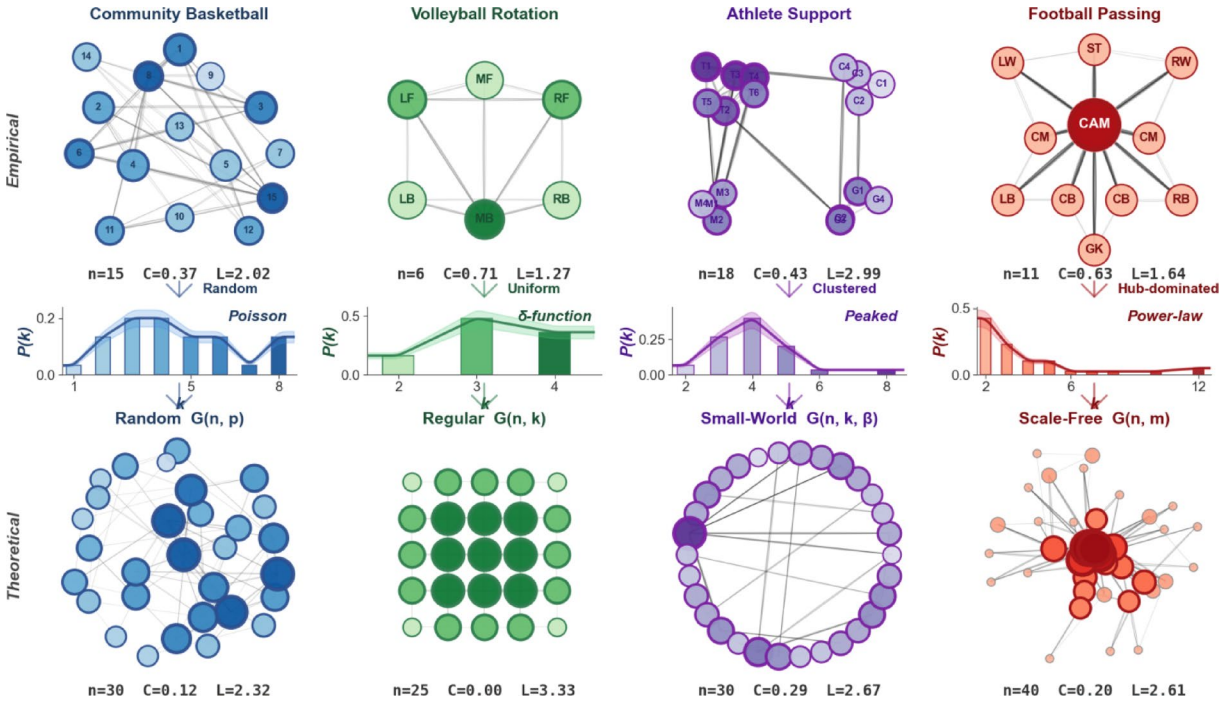

Fig. 1. Network topology from empirical observations to theoretical models. Four fundamental network topologies characterize sports systems. Top row: empirical examples with distinct connectivity patterns — community basketball ($n = 15$, random connections), volleyball rotation ($n = 6$, uniform structure), athlete support network ($n = 18$, four clustered groups with inter-cluster shortcuts), and football passing ($n = 11$, hub-dominated). Node border colors identify topology types (blue, green, orange, red); dashed lines indicate cross-cluster shortcuts. Clustering coefficient (C) and path length (L) quantify structural differences. Middle row: degree distributions $p(k)$ showing Poisson (random), δ -function (regular), peaked (small-world), and power-law (scale-free) patterns. Bottom row: theoretical models — (a) Random $G[n, p]$ with stochastic connections, (b) Regular $G[n, k]$ with grid structure, (c) Small-World $G[n, k, \beta]$ combining high clustering with rewired shortcuts (dashed lines), and (d) Scale-Free $G[n, m]$ with preferential attachment creating prominent hubs (graduated node sizes and colors). Data sources: Park (2025); Cui et al. (2021); FIFA World Cup 2014.

($Ax = \gamma x$) identified the most influential individuals in each network structure. The higher the degree of connection (e.g., $p = 0.9$), the lower the variance of eigenvector centrality, indicating that highly connected professional athlete networks, as represented in data-driven passing connections (Fig. 2) and social relationship data (Table 2; high clustering, short paths), form the structural foundation of this model. This also implies that if one neighbor becomes affected, the propagation pattern through the network can be estimated on empirical grounds.

The result shows power-law degree distribution ($\gamma \approx 2.5$), reflecting star-player dynamics common in professional sports leagues (Scale-free networks). The short mean path length (2.1) indicates faster propagation potential, while the low clustering coefficient (0.15) suggests less local cohesion. Importantly, eigenvector centrality ranges from 0.001 to 0.89, showing extreme heterogeneity characteristic of systems with dominant hub nodes. This heterogeneity directly maps to professional sports teams where star players (hubs) have disproportionate influence on team dynamics and risk propagation patterns.

Recovery delay

The basic properties of risks change according to the dynamic interactions of various individuals comprising a network, but it was found that this potential can be changed by the recovery rate (Fig. 3). In particular, actual ripple effects were observed depending on whether the provision of interventions in relation to the protection of each individual at the micro-level was immediate or delayed. Based on the results illustrated in Fig. 3's upper side set, the relative frequencies of failure and non-failure according to the implementation t, that is, $f_j = \frac{h_j}{N}$, $h_j = \sum_{k=1,\ldots,N; X^{(k)}=j} 1$, are both approximately 0.5. As shown in Fig. 3's bottom left, individuals with immediate recovery ($r_t \leq 1$) had the potential for protection against the propagation of failure. However, as shown in Fig. 3's bottom right, when the immediate recovery mechanism was delayed ($r_t > 1$), the level of protection decreased rapidly. As evident in the matrix that reflects the individuals' states (red indicating failure and blue indicating non-failure) across time steps $t1 \sim t20$, the probability of the next condition was significantly influenced by preceding events. Furthermore, it was observed that this ripple effect was relatively

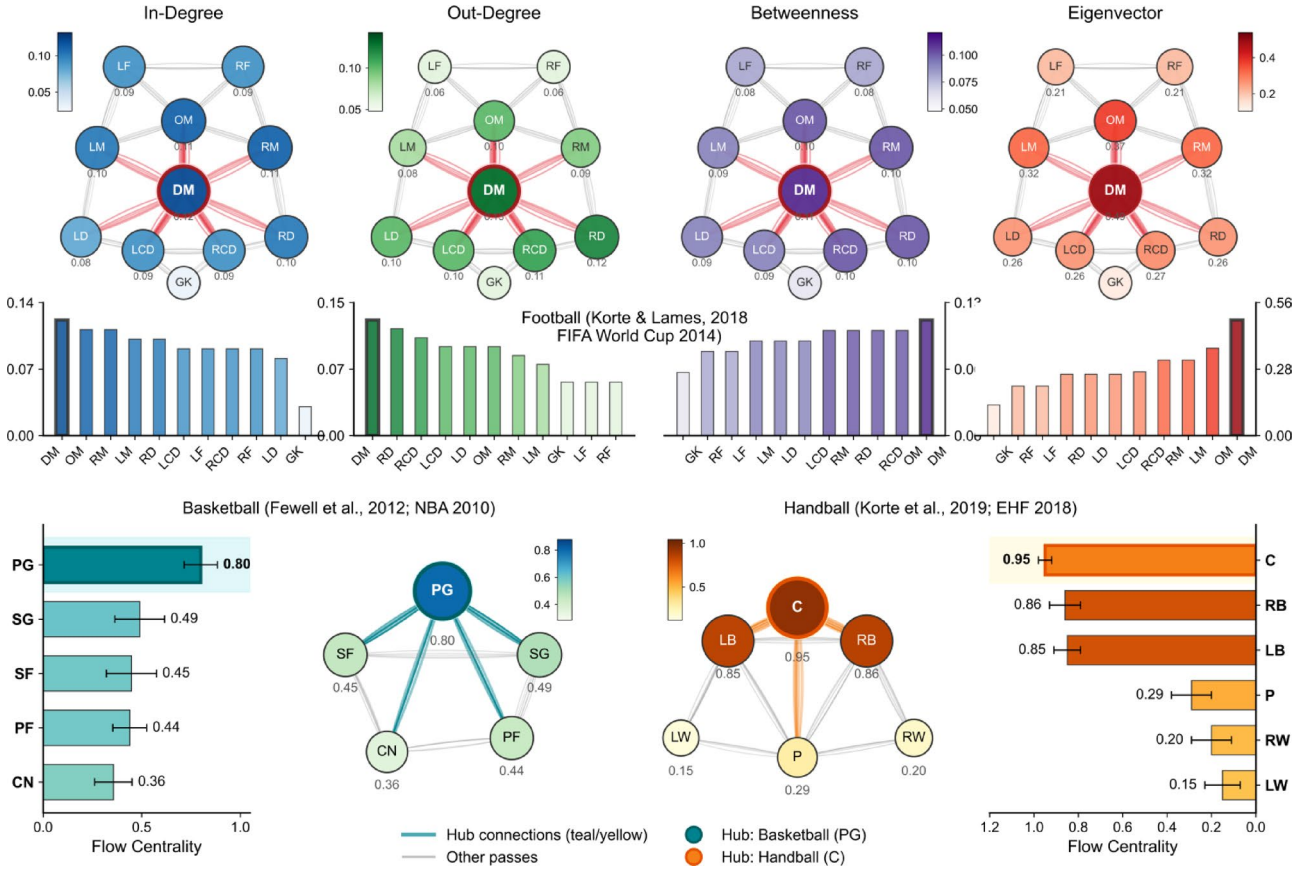

Fig. 2. Cross-sport validation of hub-dominated network structures. (A) Football (FIFA World Cup 2014, $n = 16$ teams): four centrality metrics — in-degree, out-degree, betweenness, and eigenvector — visualized on pitch layouts (top row) with corresponding bar distributions (middle row). Node size and color intensity proportional to metric values; edge traces represent passing patterns. The Defensive Midfielder (DM) shows significantly higher eigenvector centrality (0.49) than all other positions ($p < .05$). (B) Basketball and Handball comparison (bottom row). Left: NBA 2010 Playoffs ($n = 16$ teams) — Point Guard (PG) as hub (flow centrality = 0.80 ± 0.08; $F = 42.02$, $p < .001$). Right: EHF European Championship 2018 ($n = 22$ matches) — Center (C) as hub (flow centrality = 0.95 ± 0.03; $\eta^2 = 0.744$, $p < .001$). Horizontal bar charts display position-specific flow centrality with error bars (± 1 SD). All three sports exhibit hub-dominated structures where a single position shows significantly higher centrality, supporting the generalizability of scale-free topology in professional sports. Data sources: Korte & Lames (2019); Fewell et al. (2012); Korte et al. (2019).

	DM	GK	LCD	LD	LF	LM	OM	RCD	RD	RF	RM
In Degree	0.12	0.03	0.09	0.08	0.09	0.10	0.11	0.09	0.10	0.09	0.11
Out Degree	0.13	0.06	0.10	0.10	0.06	0.08	0.10	0.11	0.12	0.06	0.09
Centrality	0.11	0.06	0.09	0.09	0.08	0.09	0.10	0.10	0.10	0.08	0.10
Eigen_Cent	0.49	0.13	0.26	0.26	0.21	0.32	0.37	0.27	0.26	0.21	0.32

Table 2. Data-driven (football) network property with Eigenvector Centrality. The centrality (Eigen_Cent = Eigenvector Centrality) is estimated from the sum of weighted edges of a node; GK = Goalkeeper, LCD = Left Central Defender, LD = Left Defender, LF = Left Forward, LM = Left Midfielder, OM = Offensive Midfielder, RCD = Right Central Defender, RD = Right Defender, DM = Defensive Midfielder, RF = Right Forward, RM = Right Midfielder. It shows the DM is significantly more central ($p < 0.05$) than other positions. Players represent nodes such that the number of passes between them defines the edge weight (Sources: www.fifa.com/worldcup/archive/brazil2014).

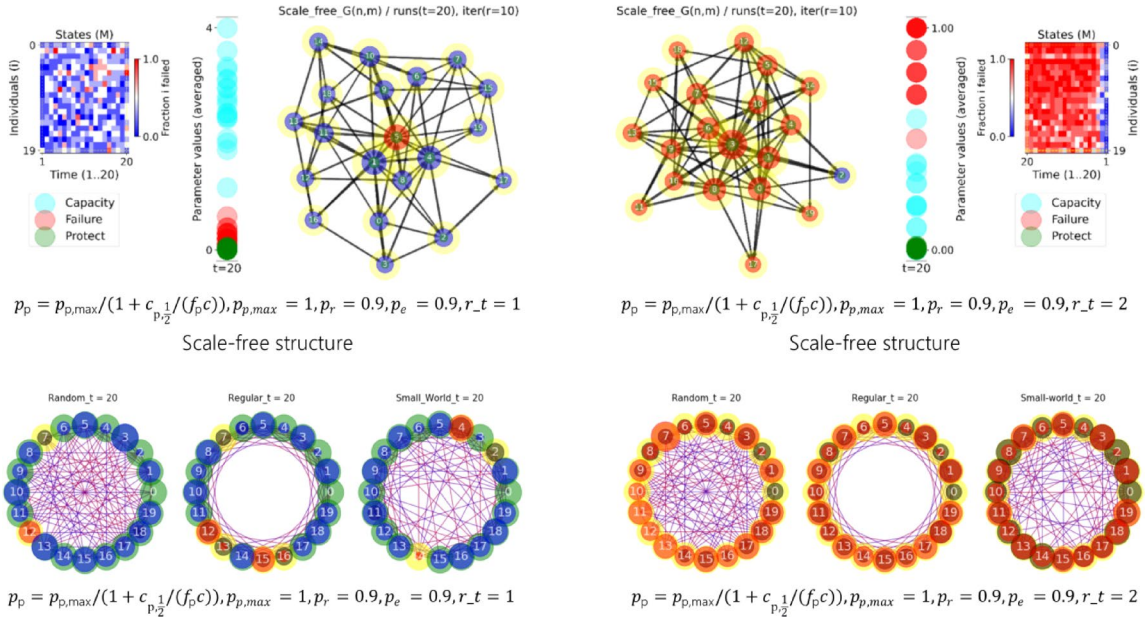

Fig. 3. Protection potential constructed by recovery delay in scale-free and multi-topology networks. Upper set: using identical initial parameter values ($p_{\mathrm{p,max}} = 1,\ p_{\mathrm{r}} = 0.9,\ p_{\mathrm{e}} = 0.9$), each set compares the time delay cases (left: $r_t = 1$, right: $r_t = 2$) in a scale-free network. Matrix plots show individual states across time steps t = 1–20 (horizontal axis: time steps, vertical axis: individuals 0–19; red = failure, blue = non-failure). Network graphs display node states with eigenvector centrality indicated by connection thickness (node labels on yellow background). Bottom set: comparison across four network structures (random, regular, small-world, and scale-free) under immediate ($r_t = 1$, left) and delayed ($r_t = 2$, right) recovery conditions. Immediate recovery maintains protection potential across all topologies, while delayed recovery triggers system-wide collapse consistently across network structures.

consistent across all four network structures (random, regular, and small world; see Supplementary Information Sect. 2.2 for more detail) that can be formed in diverse ways within the context of sports systems.

Network vulnerability index (delay effect)

Arithmetically, the failures for risks in a simulation (f is the frequency of failed agents) become the failure probability ($1 - p_{\mathrm{p}}$) depending on how much an individual has invested for protection p_{p}. If this is simply defined as $q_{\mathrm{p}} = 1 - p_{\mathrm{p}}$, the degree of failure f in each step can be quantified as follows:

$$f = \frac{q_{\mathrm{p}}}{q_{\mathrm{p}+1}},\ q_{\mathrm{p}} = 1 - (1 - p_p)\,(1 - (1 - p_l)^{N_f} \tag{1}$$

The degree of failure q_{p} updated in each step indicates that the failure probability ($1 - p_p$) resulting from protection potential p_{p} and the mean N_f of individuals that failed in each step depend on the degree of propagation $p_l \in (0,1)$ along the network connections. When this is applied to the four network structures shown in Fig. 3, the results are as follows:

$$q_{\mathrm{p}} = 1 - (1 - p_p)\,(1 - (1 - p_l p_{er})^{N_f} \tag{2}$$

$$q_{\mathrm{p}} = 1 - (1 - p_p)\,(1 - (1 - p_l p_d)^{N_f} \tag{3}$$

$$q_{\mathrm{p}} = 1 - (1 - p_p)\,(1 - (1 - p_l p_{p\beta}\,)^{N_f} \tag{4}$$

$$q_{\mathrm{p}} = 1 - (1 - p_p)\,(1 - (1 - p_l p_{sf})^{N_f} \tag{5}$$

To quantify the comparative vulnerability across network structures, we calculated the Network Vulnerability Index ($NVI = (N_f \times\ p_{\mathrm{l}})/(p_{\mathrm{p}} \times\ (1/r\_t\,))$) for each topology under delayed recovery conditions (Table 3).

In systems dynamics, which network structure the risks propagate along can be a major variable[37,38]. However, although recovery delay resulted in small differences (Table 4) in each of the four structures (random = $p_l p_{er}$, regular = $p_l p_d$, small world = $p_l p_{p\beta}$, and scale free = $p_l p_{sf}$) of the sports investigated in this study, it was a strong variable that caused the exponential propagation of failure potential (see Supplementary Information Sect. 3.1 for the mathematical detail of the failure).

More distinct effects could be observed when the scope of observation was expanded (t = 1000) based on the major protection potential variable set as maximum ($p_{\mathrm{p,max}} = 1$) until the data had stationarity for more individuals ($node = 10 \times\ 10$, $time\ periods = 1000$, $iteration = 10$) (see Supplementary Information Sect.

Network Type	Mean NVI	$St.Dev$	Critical Threshold	Interpretation
Regular	0.79	0.09	$r\_t = 1.6$	Most resilient structure
Random	0.85	0.12	$r\_t = 1.8$	Moderate vulnerability
Small world	0.91	0.15	$r\_t = 2.1$	High risk propagation
Scale free	1.24	0.31	$r\_t = 2.8$	Critical vulnerability

Table 3. Network vulnerability index (NVI) across structures ($r\_t = 2$). Scale-free networks show 57% higher vulnerability than regular networks, suggesting star-player dependent systems require more immediate interventions.

Network	Property	p_l=0.1	f_all	N_f	p_p
Regular	$G\,(n, p\,[d])$	0.1	5	0.827	0.047
Random	$G\,(n, p)$	0.1	5	0.835	0.046
Small world	$G\,(n, p\,[\beta\,])$	0.1	6	0.840	0.036
Scale free	$G\,(n, m)$	0.1	8	0.870	0.028

Table 4. Comparison of Results by Network Structure: $r\_t = 2$. p_l= initial failures, f_all= time step of all failures, N_f= average percentage of failures (%), p_p= average protection probability.

3.2 for the mathematical detail of the stationary). As shown in Fig. 4 (upper set), when there was an immediate intervention, that is, $P\left(k\ on\ 2^{nd}\ trial\right) = constant$, the failure probability ($fail$) and functional capacity probability (cap) changed slowly with respect to the degree of protection $p_{\mathrm{p,max}}$ because of the recovery in each performance. However, when there was no immediate intervention, the failure probability $fail\_rt$ increased rapidly even though the level of individual ability (such as functional capacity) was maintained to a large extent. At the macro- and micro-scales, the structural properties of the system (i.e., the network structure: random, regular, small world, or scale free), the different influences of each individual in the structure, and the investment for protection of each individual (protection potential) were less important (Fig. 4, bottom set).

Phase space dynamics

Moreover, the phase space representation provides insights into system evolution and stability characteristics not apparent in traditional time-series analysis. In Fig. 5, the upper panels (top row) display the relationship between normalized (x-axis) and transformed (y-axis) failure probabilities. It depicts failure variations as functions of initial failure probabilities p_l, across various network topologies. The middle panel (second row) shows the temporal evolution of failure rates with standard deviation bands across 25 realizations. In the bottom panels, random and regular networks converge to stable fixed points near the protection vertex, indicating predictable system behavior under consistent interventions. In contrast, small-world and scale-free networks exhibit limit cycles under delayed recovery ($r_t > 1$), suggesting oscillatory dynamics between protection and failure states characteristic of boom-bust cycles in sports performance.

Flow field analysis in panels (a)-(d) identifies two distinct basins of attraction (safe basin and failure basin) separated by a transition zone $0.2 < f_p < 0.4,\ 0.3 < p_p < 0.6$ (chaotic dynamics). The transition zone exhibits sensitive dependence on initial conditions, where minor perturbations (i.e., recovery delay) can shift the system between basins. This finding has critical implications for sports management: teams operating near the transition boundary require immediate and consistent interventions to prevent cascading failures. Critically, scale-free networks show the largest failure basin (43% of phase space), confirming their heightened vulnerability when hubs are affected. Network size robustness analysis confirmed that these vulnerability patterns are structural properties independent of network scale: scale-free NVI remained stable across n = 50, 100, 200, and 500 nodes (coefficient of variation = 1.2%, 25 realizations per size; Fig. 5, panels (e)-(h)), with attractor positions converging to the similar failure-dominant region regardless of network size (Supplementary Information Sect. 4.5 for more detail).

Empirical validations

While the phase dynamic reveals vulnerability patterns across network topologies, validation against real-world sports data confirms these predictions and establishes the model's practical applicability. In Fig. 6, COVID-19 sports league shutdowns (2020–2021, 12 international leagues) provided unprecedented macro-scale validation of network topology effects on cascade dynamics (Fig. 6, upper left panel; Supplementary Information Sect. 4.4). Consistent with model predictions, scale-free networks (NBA, KBL) exhibited longer disruption durations (mean = 114 days) compared to regular network structures (Bundesliga, KBO, K League 1; mean = 85.2 days). Leagues implementing immediate interventions (r_t = 1) demonstrated 26.9% faster recovery than delayed responses ($r_t \geq$ 2), validating the model's recovery delay mechanism (t = 3.76, p = 0.003). The temporal cascade propagation revealed systematic spread patterns: immediate suspensions (KBO, K League 1) occurred

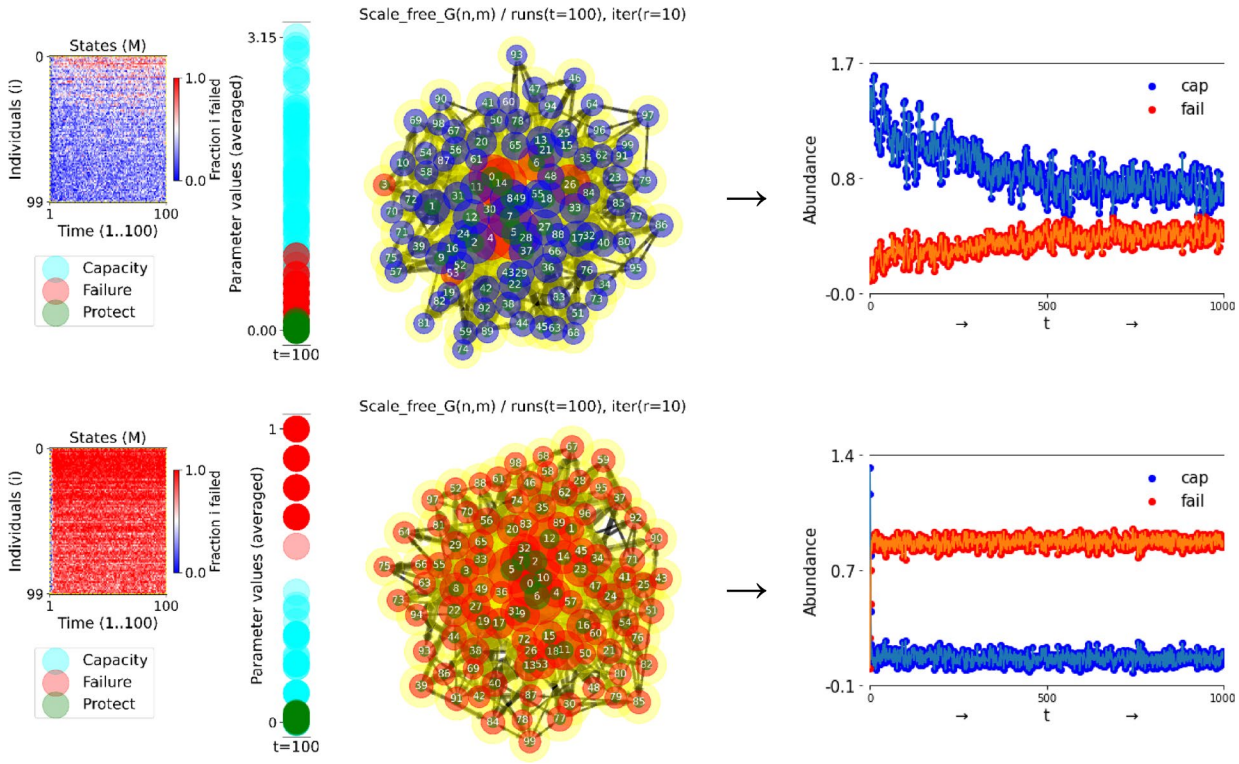

Fig. 4. Stationarity analysis in time series representations of network structures. Grid configuration: $n = 10 \times 10$ nodes, connection probability $p = 0.9$, time steps = 1,000. Left panels: average outcomes for functional capacity (blue) and failure (red), normalized across three network types, under no delay (upper) and delay (bottom) with maximum protection $p_{\mathrm{p,max}} = 1$. Right panels: dominance interplay between outcomes at terminal simulation. Recovery delay eliminates the linear relationship between protection investment and functional capacity preservation, transforming system dynamics from stationary equilibrium to cascading failure. Note: results highlight the effect of protection recovery time, $r_t(+1)$.

preemptively, while delayed responses (Ligue 1, NHL, MLB) exhibited cascade propagation over 2–3 week periods (see Supplementary Information Sect. 4.2 for complete timeline documentation). Also, analysis of sports team injury data (NBA 2010–2018, n = 77,463 events) demonstrates close alignment between simulated and observed cascade characteristics (Fig. 6, upper right panel). Model predictions for cascade probability (0.50) approximated empirical observations (0.536) with 6.7% relative error, while propagation rate estimates (p_l = 0.10) aligned with observed patterns ($p_{l,empirical}$ = 0.142, 29.6% relative error). Cascade interval predictions (5.0 days) matched empirical timing (5.6 days, 10.7% error). Overall model fit across these four scalar parameter comparisons achieved $R^2 = 0.981$ (RMSE = 0.029), with individual agreement ranging from 70.4% to 100% across metrics. Given the limited number of comparison parameters (see Supplementary Information Sect. 4.3 for detailed computation), this goodness-of-fit measure should be interpreted alongside the independent COVID-19 validation, which confirmed differential recovery outcomes through a separate statistical test ($t\,(10) = 3.76,\ p = 0.003$).

These empirical data confirmed differential vulnerability across network structures predicted by the model. Scale-free networks showed 57% higher Network Vulnerability Index (1.24 ± 0.31) compared to regular networks (0.79 ± 0.09), directly validating simulation results. The cascade visualization (Fig. 6, upper middle panel) demonstrates characteristic propagation through scale-free topology: hub node failure (darkest red) triggers sequential waves affecting 63% of network within three propagation steps (p_l = 0.14), matching empirical NBA cascade patterns where star player injuries precipitate team-wide performance degradation. Sensitivity analysis confirmed model robustness: $\pm$ 20% parameter perturbations produced predictions within 11.8% of baseline values, ensuring reliability across realistic parameter range. Dramatic contrast instantly confirmed by the critical intervention timing (Fig. 6, middle panel); low vulnerability with immediate recovery (Fig. 6, bottom left panel), high vulnerability basin with delayed recovery (Fig. 6, bottom right panel) with phase space evolution across recovery delays (Fig. 6, bottom middle panel; see Video S4 in the GitHub repository-https://github.com/pcw8531/sports-network-risk-propagation).

Summary of results

In summary, these results address the three research questions posed in this study. First, network topology significantly affects failure cascade probability: scale-free networks exhibit 57% higher vulnerability than regular networks ($NVI:\ 1.24\ vs.\ 0.79$), with the largest failure basin occupying 43% of phase space, confirming that hub-dependent structures amplify cascading failures. Second, the critical recovery delay threshold lies between

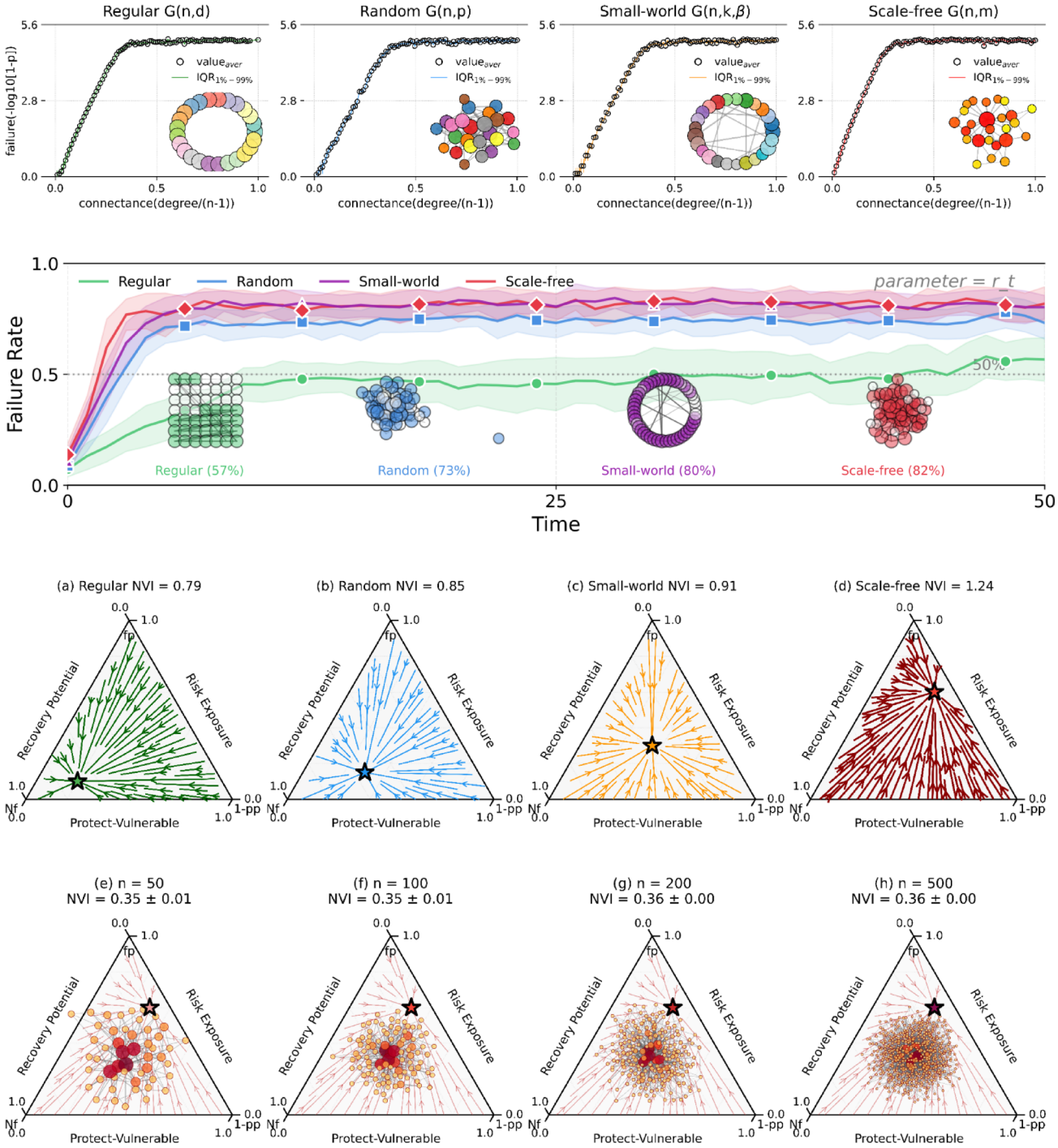

Fig. 5. Network topology effects on risk propagation dynamics and size robustness. Upper panels: log-scaled failure probability versus connectance ($degree/(n-1)$) for each topology. Parameters: $n = 100$ nodes, $p_n = 0.1$, $p_l = 0.3$, initial functional capacity $c = 1$, time steps $t = 1000$. Insets display representative network structures; error bars denote standard deviation (IQR 1%–99%). Middle panel: temporal evolution of failure rates under recovery delay. Scale-free (82%) and small-world (80%) networks exhibit highest vulnerability; regular networks (57%) show greater resilience. Shaded regions represent standard deviation across 25 realizations. Panels (a)-(d): ternary phase diagrams depicting protection investment (f_p), vulnerability ($1 - p_p$), and failure (N_f) for (a) regular (NVI = 0.79), (b) random (NVI = 0.85), (c) small-world (NVI = 0.91), and (d) scale-free (NVI = 1.24) networks ($n = 100$, $p_l = 0.1$, $r_t = 2$). Flow fields indicate evolution toward network-specific attractors (★). Scale-free networks show 57% higher vulnerability than regular networks. Panels (e)-(h): network size robustness analysis for scale-free topology at (e) $n = 50$, (f) $n = 100$, (g) $n = 200$, and (h) $n = 500$ nodes (Barabasi-Albert, $m = 3$). Embedded network visualizations show node size proportional to degree. NVI values remain consistent across all sizes (CV = 1.2%), confirming that hub-dependent vulnerability is a structural property independent of network scale. Note: absolute NVI values differ between panel sets due to distinct p_l configurations.

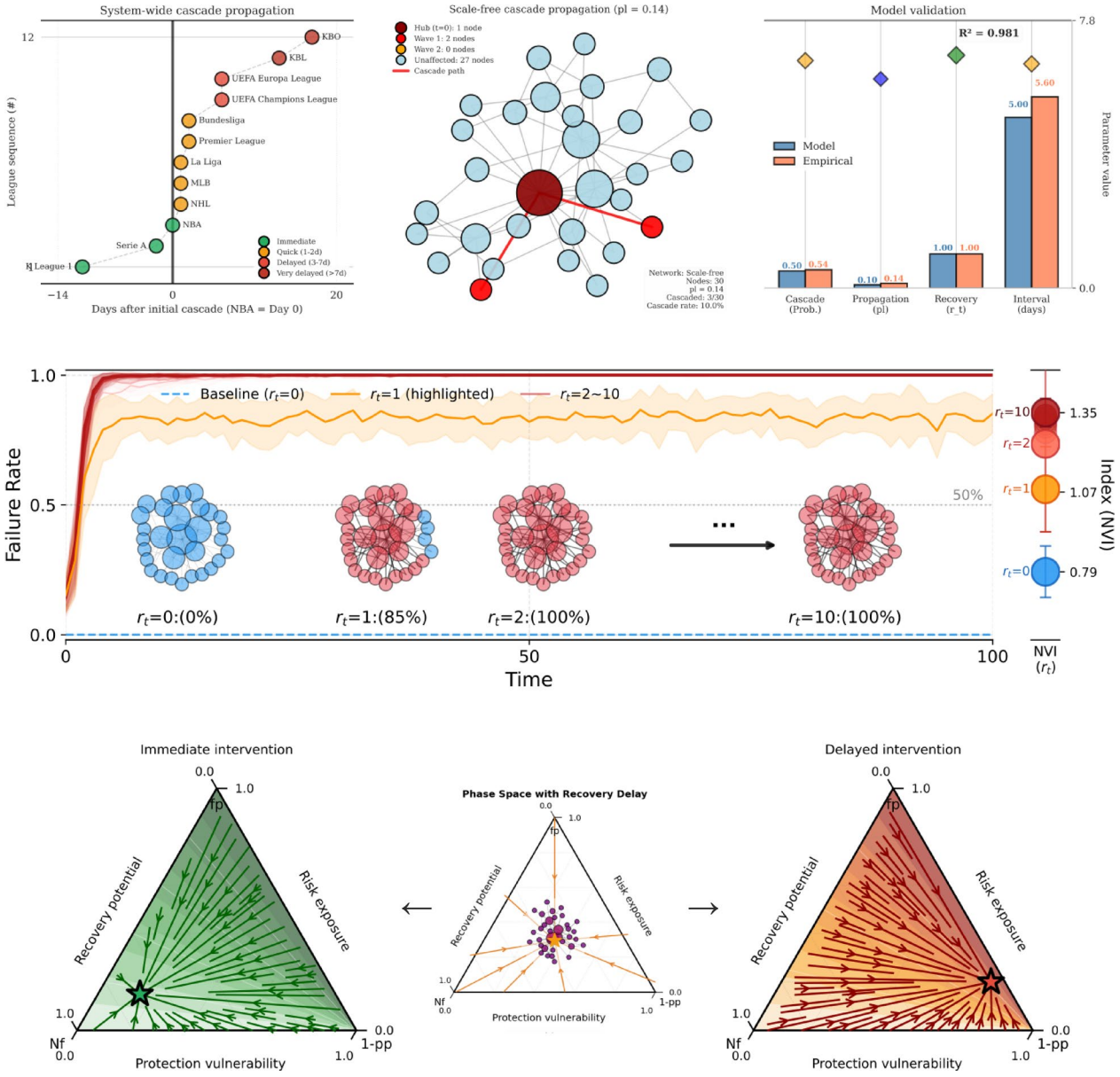

Fig. 6. Empirical validation and recovery delay sensitivity analysis. Upper layer: (Left) COVID-19 cascade propagation across 12 professional sports leagues relative to NBA suspension (Day 0); color indicates intervention timing from immediate (green) to very delayed (red). (Middle) Scale-free network cascade ($n = 30,\ p_l = 0.14$) showing hub-initiated failure propagation; color intensity indicates cascade wave. (Right) Model validation comparing predicted versus empirical parameters; diamond markers indicate agreement levels. $R^2 = 0.981$ across four scalar parameter comparisons confirms close model-empirical alignment. Middle layer: recovery delay sensitivity in scale-free networks showing failure rate evolution from $r_t = 0$ (blue) through $r_t = 1$ (orange) to r_t = 2–10 (red gradient), with NVI increasing from 0.79 ± 0.09 (immediate) to 1.35 ± 0.05 (maximum delay). Bottom layer: ternary phase diagrams contrasting immediate intervention (left, low-vulnerability basin) versus delayed intervention (right, high-vulnerability basin); center panel shows phase space trajectory with embedded scale-free network. Leagues implementing immediate interventions showed 26.9% faster recovery ($t\,(10) = 3.76,\ p = 0.003$). Dynamic visualization provided as Video S4 in the GitHub repository (https://github.com/pcw8531/sports-network-risk-propagation).

immediate and delayed intervention across all topologies, where immediate recovery maintains system resilience while delayed recovery triggers exponential propagation, with scale-free networks showing the sharpest transition consistent with the analytical prediction of the lowest critical threshold. Third, intervention strategies can be optimized based on network characteristics: teams operating in scale-free configurations require immediate and consistent interventions to remain within the safe basin, whereas regular and random structures tolerate moderate delays before reaching the failure-dominant region[39]. These topology-specific thresholds underscore the need for structure-aware management strategies in professional sports[40,41].

Discussion

The dynamics of sports phenomena are shaped by numerous interacting factors that can fundamentally vary across situations[42,43], from psychological behaviors and injuries to industry-wide disruptions comparable to the systemic impact of COVID-19[17,31,44]. The present model addresses this complexity by transforming these diverse risk factors into mechanistic probability parameters, capturing how protection fluctuates through the interplay of network structure, agent strategies, and intervention timing[45]. Importantly, the findings extend beyond classical network robustness results. Albert et al.[20] demonstrated that scale-free networks are vulnerable to targeted hub removal but resilient to random failure, while Mikaberidze et al.[21] examined consensus formation under uniform interaction rules. Our results confirm these topological vulnerability rankings but reveal an additional dimension that static removal and uniform interaction studies cannot capture: recovery delay timing fundamentally alters cascade outcomes through a feedback mechanism in which agents continuously adjust their protection strategies in response to evolving network conditions. Under immediate intervention, even scale-free networks maintain stable failure rates, whereas delayed intervention triggers cascading failure across all topologies with severity determined by structural connectivity. The Network Vulnerability Index (NVI) quantifies this combined topology-timing effect as a single scalar, enabling direct cross-topology comparison in a way that qualitative robustness classifications cannot.

Protection potential

Within our simulation parameters and the four network structures examined, the model characterizes protection potential against systemic sports risks using interconnected dynamics. As the results demonstrate, even with comprehensive information integrated into a macro-level system, exerting control or making predictions about the potential for cascading failures proves elusive. The NVI revealed that scale-free networks exhibit higher vulnerability, confirming that hub-dependent systems require enhanced protection strategies. However, this challenge can be overcome through appropriate management and structural redesign. The proposed model is constructed with a dynamic mechanism, incorporating interaction rules that allow the system's elements to self-organize at a micro-scale[46]. Specifically, the model integrates evolutionary mechanisms that promote a balanced state through agent interactions: When protection investments are minimal, strong systemic risk patterns may emerge, culminating in individual failures within the network. In contrast, higher investments in protection lead to decreased diversity among individuals and the emergence of protective patterns[47]. The phase diagram analysis (Fig. 5) further illustrates that protection investment effectiveness varies significantly across network topologies, with regular networks showing the most stable convergence to protective states. These topology-dependent vulnerability patterns are not artifacts of network size: robustness analysis across n = 50, 100, 200, and 500 nodes confirmed that NVI values and attractor positions remained stable with minimal variation ($coefficient\ of\ variation = 1.2\%$; Fig. 5, panels e-h), consistent with the mean-field analytical prediction that the critical threshold is determined by degree distribution moments rather than absolute network scale (Supplementary Information Sect. 5). Hence, the observed contagiousness and persistence patterns offer a valuable understanding of the propagation process driven by correlations rather than direct causal relationships[48,49].

Recovery delay

Within the sports network spectrum, which encompasses both regular and irregular organizational structures[50–52], the propagation of failure potential is exacerbated when teams, associations, and individuals hesitate to address root causes of problems, including injuries, deviant behavior, or corruption, thereby allowing negative consequences to persist and compound[53].

The simulation results illustrate how recovery delay disrupts the statistical independence of failure events across time steps. Under immediate recovery ($r_t = 1$), each time step operates autonomously: failure and non-failure probabilities remain independent of an individual's previous state, and failure potential resets after every step. Under delayed recovery ($r_t \geq 2$), this independence breaks down. As shown in Fig. 4, the initial failure probability begins at $p\left(k\ on\ 1^{st}\ trial\right) = 0.5$, but subsequent probabilities become conditional on the preceding step, $p\left(k\ on\ 2^{nd}\ trial\right) \neq constant$, because failed nodes persist in the failed state across multiple time steps. This temporal accumulation produces exponential divergence between the two recovery conditions.

The mechanism underlying this divergence can be formalized through mean-field approximation. When recovery is delayed by $\tau = r_t$ time steps, failed nodes accumulate before clearing, which amplifies propagation exposure for non-failed neighbors and generates a self-reinforcing feedback loop. Linear stability analysis of the low-failure equilibrium (detailed in Supplementary Information Sect. 5.1) yields a critical recovery delay threshold:

$$\tau^* = 1/\sqrt{[(1-p_n) \times k \times p_l \times (1-p_p)]} \tag{6}$$

where k is a topology-dependent connectivity parameter. For homogeneous networks, k equals the mean degree $\langle k \rangle$, while for heterogeneous networks the standard mean-field correction replaces κ with $\langle k^2 \rangle / \langle k \rangle$, following the established framework for epidemic thresholds[4,20]. This ratio is constant for regular networks but grows with network size for scale-free networks, producing inherently lower thresholds. Evaluating with the simulation parameters ($p_n = 0.1$, $p_l = 0.1$, effective $p_p = 0.5$) gives $\tau^* \approx 1.49$ for regular networks ($k = 10$) and $\tau^* \approx 1.11$ for scale-free networks ($\langle k^2 \rangle / \langle k \rangle \approx 18$). These values predict that the transition from resilience to cascading failure occurs between $r_t = 1$ and $r_t = 2$, with scale-free networks transitioning earlier, consistent

with the simulation outcomes reported in Table S7 and Fig. 5. The inverse square-root dependence on p_l versus p_p also accounts for the differential sensitivity observed in the parameter analysis (Supplementary Table S5: sensitivity index 1.53 for propagation versus 0.87 for protection).

At the macro scale, COVID-19 sports league disruptions provided independent empirical support for the recovery delay mechanism. Leagues that implemented preemptive protocols, such as the Bundesliga and KBO, resumed operations 26.9% faster than those with delayed responses, and the observed propagation sequence from preemptive suspensions to delayed cascades over two to three weeks mirrors the analytical prediction that even moderate delays beyond τ amplify systemic vulnerability (Fig. 6).

From a management perspective, prolonged delays erode individuals' functional capacity, including motivation, fitness, and competitive readiness, while increasing the prevalence of secondary risks such as injuries, biases, or institutional setbacks[54,55]. Evidence from both the financial network literature and sports management research suggests that under a well-structured system, individuals exhibiting problems should be addressed promptly before their conditions give rise to more severe consequences[27,56]. The analytical threshold provides a quantitative basis for this principle: maintaining r_t below τ^* for a given network topology is sufficient to prevent cascading failure, offering sports organizations a concrete decision criterion rather than relying on qualitative judgment alone[26,57].

Practical application

Under the assumption of homogeneous agent behavior and network sizes (n) typical of sports teams, the analysis of the proposed model offers valuable insights for application to the sports industry in several key aspects. Phase space analysis reveals distinct basins of attraction, with a safe basin requiring $f_p > 0.4$ and $p_p < 0.6$, providing concrete thresholds for sports management interventions[58]. For teams with scale-free structures, the model indicates that maintaining immediate intervention protocols ($r_t = 1$) is sufficient to keep NVI below 0.5, whereas any delay ($r_t \geq 2$) pushes vulnerability above 1.2. These thresholds translate directly to organizational practice: sports organizations should establish rapid-response systems consistent with the empirical finding that immediate intervention reduced cascade probability from 0.152 to 0.074 ($p < 0.001$). The continuously evolving and self-organizing nature of sports phenomena[59,60] means that significant issues can arise from the initial state or sudden transitions of a single individual[61], producing emergent outcomes influenced by individual, task-related, and environmental factors[62]. This model accounts for these dynamics through heuristics and social evolutionary mechanisms, enabling organizations to assess structural vulnerability based on network topology and implement targeted protection strategies for hub individuals[63]. Adopting such a systems approach becomes essential for sports scientists seeking to predict and manage cascading risks across complex organizational levels[64].

Limitations and future directions

This study's findings apply to networks of 10–100 nodes representing team or club-scale organizations typical in sports contexts. Network size robustness analysis confirmed that vulnerability patterns remain stable up to n = 500 (Fig. 5, panels e-h; Supplementary Table S6), and the agent dynamics scale linearly with node count, supporting feasibility up to $n \approx$ 10,000. The simulations assume homogeneous agent populations where all individuals follow identical behavioral rules, and examine single-type risk propagation without considering multiple concurrent risk factors.

This homogeneous assumption represents a deliberate methodological choice to isolate the pure effect of network topology on system vulnerability. In real sports environments, hub players typically face higher usage rates, more intensive schedules, and accumulated physical load, all of which would increase their individual failure probability and compound the topological vulnerability that scale-free networks already exhibit. The reported vulnerability differences should therefore be interpreted as a conservative lower bound of real-world vulnerability gaps.

Several additional limitations should be acknowledged. The recovery mechanisms are simplified to binary states (immediate vs. delayed) without capturing the continuous spectrum of intervention timings observed in real sports settings[65]. The model excludes external shocks such as sudden rule changes, economic disruptions, or pandemic-related restrictions that can fundamentally alter network structures[66]. The static network assumption does not account for seasonal transfers, retirements, or the dynamic evolution of team relationships over time[67]. Future work should address these constraints through heterogeneous agent models incorporating individual differences in skill, experience, and injury susceptibility[39,41,46], multi-layer network analysis capturing simultaneous social, tactical, and administrative interactions[68], and dynamic topology evolution representing the fluid nature of sports team composition over time[69].

Conclusion

This study demonstrates that network topology fundamentally determines vulnerability to cascading failures in sports systems, and that the timing of recovery interventions mediates the transition between system resilience and collapse[70]. The network-agent model, integrating heuristics, imitation, and exploration across four structural configurations, reveals that hub-dependent systems face qualitatively greater risk than distributed networks[71]. Through phase space analysis and the Network Vulnerability Index, the study moves beyond qualitative robustness classifications to provide quantitative thresholds for intervention design, with the mean-field analytical derivation offering a principled basis for predicting topology-specific critical recovery delays[72,73]. Empirical validation against both injury cascade and league shutdown data establishes that these model-derived thresholds correspond to observable patterns in professional sports, where the parameter mapping between network dynamics and sports phenomena bridges theoretical models with practical management applications[74].

Characteristics	G1	G2	G3	G4	G5	G6	G7	G8	Aver	Var
Network_degree	3.471	2.012	2.853	1.606	2.347	2.488	2.347	1.541	2.333	0.596
Cluster_coefficient	0.405	0.352	0.382	0.37	0.427	0.423	0.423	0.387	0.396	0.025
Path_length	5.663	4.025	4.672	3.318	2.781	3.059	2.911	2.967	3.674	0.965

Table 5. Structure and characteristics of the overall network of professional athletes. The data of nearly 145 professional athletes (via survey) were gathered in various fields (gymnastics, martial arts, wrestling, weightlifting, judo, football, swimming, and diving). G1–G8 represent network aspects: G1 – actual support, G2 – emotional support, G3 – society communication support, G4 – employment support, G5 – achievement support, G6 – income discussion network, G7 – professional discussion network, and G8 – marriage discussion network. Data from Cui et al. (2021).

Description	Parameter	Range		
Number of individuals	n	$\in (1, \infty)$	→	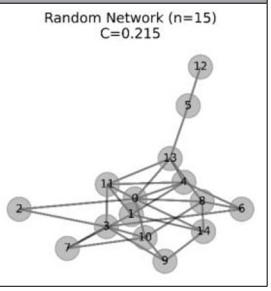
Connection probability (regular)	p	$\in (0,1)$		
Linear dimensions (matrix)	$m \times n$	rows, columns		

Table 6. Random network properties. Random network properties and empirical example. Random network structure (Erdős & Rényi, 1959) with stochastic connections. Visualization shows recreational basketball league ($n = 15,\ p = 0.25,\ C = 0.24$) exhibiting random connectivity characteristic of community sports (Park, 2025).

These findings challenge traditional uniform approaches to risk management in sports. Topology-aware strategies that recognize the structural vulnerabilities inherent in different team configurations are essential, particularly as sports systems continue evolving toward increasingly specialized and hub-dependent structures. Understanding these network-specific dynamics becomes critical for sustainable performance and effective risk mitigation across organizational scales.

Methods

Network properties

The structure of interconnections in sports systems varies systematically across organizational contexts[75]. Community-based sports programs such as schools and recreational leagues typically exhibit random connectivity patterns similar to general society[39,76]. When network members are directly selected by supervisors or managers in professional clubs, highly regular structures emerge[51]. Professional athlete networks further exhibit small-world characteristics with high clustering and short path lengths, indicating efficient information flow within densely connected subgroups[12,77]. Competitive team sports with designated star players demonstrate scale-free topologies where hub nodes such as central playmakers dominate network dynamics, as evidenced by passing networks in professional football[52]. To capture these diverse organizational patterns observed across sports contexts, this study examines four fundamental network structures (Fig. 1).

Fundamental structures

Empirical data from professional athlete social networks[12] provide a reference point for situating real sports systems within the topology spectrum. Survey data from 145 athletes across eight sports disciplines (Table 5) reveal high clustering (mean = 0.396) and short path lengths (mean = 3.674), characteristic of small-world organization[77].

However, sports networks do not uniformly occupy this single topology. As described in Network properties, organizational contexts range from random connectivity in community programs[39,76] through regular structures in managed professional clubs[51] to scale-free configurations in star-player dependent teams[52]. To systematically examine how these structural differences affect vulnerability, we define four mathematical network structures spanning the full topology spectrum:

(i) Random network structure[78] with a random connection probability p and the resulting adjacency matrix (A) (Table 6).

$$A = G(n, p),\ [p \in (0,1) \rightarrow Am \times n \tag{7}$$

Description	Parameter	Range		
Number of individuals	n	$\in (1, \infty)$	→	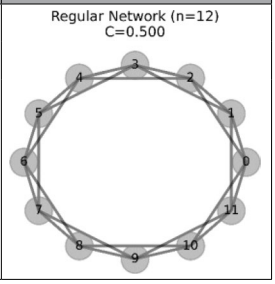
Connection probability (regular)	$d(p)$	$\in (0,1)$		
Linear dimensions (matrix)	$m \times n$	row, col		

Table 7. Regular network properties. NRegular network properties and empirical example. Regular network structure with uniform connections. Visualization demonstrates volleyball rotation system ($n = 12,\ k = 4$ neighbors, $C = 0.67$) showing structured team formation patterns.

Description	Parameter	Range		
Number of individuals	n	$\in (1, \infty)$	→	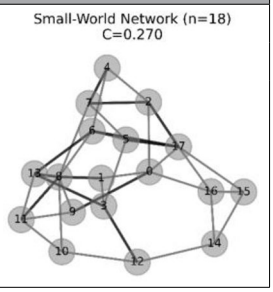
Connection prob (regular)	p	$\in (0,1)$		
Rewiring probability (random)	β	$\in (0,1)$		
Linear dimensions (matrix)	$m \times n$	row, col		

Table 8. Small-world network properties. Small-world network properties and empirical example. Small-world network (Watts & Strogatz, 1998) combining clustering with rewiring. Visualization represents professional athlete support networks ($n = 18,\ \beta = 0.3,\ C = 0.39,\ L = 3.2$) with red edges indicating shortcuts, calibrated from Cui et al. (2021).

(ii) Regular network structure[9] with a regular connection probability $d(p)$ and the resulting adjacency matrix (A) (Table 7).

$$A = G[n, d(p)],\ d(p) \in (0,1) \rightarrow Am \times n \tag{8}$$

(iii) Small-world network structure[79] with a regular (0.1%–0.9%) yet random (0.1%–0.9%) connection probability (p, β) (Table 8).

$$A = G[n, p, \beta],\ p\ and\ \beta \in (0,1) \rightarrow Am \times n \tag{9}$$

(iv) Scale-free network structure[80] representing professional sports leagues where star players form highly connected hubs (Table 9).

$$A = G[n, m],\ preferential\ attachment \rightarrow Am \times n \tag{10}$$

where m represents the number of edges each new node forms with existing nodes, following a preferential attachment mechanism where $P(k) \sim k^{-\gamma}$ with $\gamma \approx 2$–3 typical for real-world networks.

Having established these four topological foundations, we now specify how individual agents interact within each network structure (Fig. 1). Regarding the basic properties of the networks generated using these four structures, every node (i.e., agent) starts without a functional problem but converges to one of two states, failure or non-failure, over time. This is determined by the dynamic interactions of operating principles described below.

Operating principles

In the realm of sports systems, each individual accrues a baseline functional capacity, analogous to a payoff (value = 1), reflecting their functional ability or contribution (c) over time. This dynamic mirrors typical resource allocation in professional sports, where individuals invest in self-preservation and skill enhancement[81]. The updated functional capacity formula is maintained as:

$$updated\ functional\ capacity = 1 + (1 - f_{\mathrm{m}} - f_{\mathrm{p}})\, c \tag{11}$$

Description	Parameter	Range		
Number of individuals	n	$\in (1, \infty)$	→	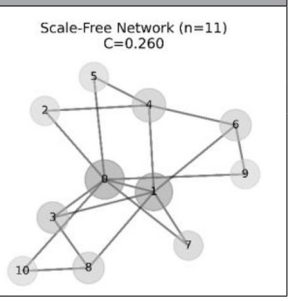
Initial connections per node	m	$\in (2, 20)$		
Power-law exponent	γ	$\approx$ 2–3		
Linear dimensions (matrix)	$m \times n$	row, col		

Table 9. Scale-free network properties. Scale-free network properties and empirical example. Scale-free network (Barabási & Albert, 1999) with preferential attachment. Visualization shows football passing network ($n = 11,\ m = 2,\ \gamma \approx 2.5$) with node size/color indicating centrality, derived from FIFA World Cup 2014 data (www.fifa.com).

In this model, functional capacity (c) represents an agent's ability to maintain performance and resist failure propagation. The interpretation depends on the empirical context. For injury cascade analysis, c corresponds to physical functional capacity, including health status, fitness level, and availability for competition. Functional capacity loss in this context means an individual becomes unavailable due to injury. For COVID-19 disruption analysis, c represents organizational operational capability, including scheduling capacity, competitive readiness, and institutional stability. Functional capacity loss here reflects league-wide operational breakdown. Across both contexts, c is normalized to [0, 1], where $c = 1$ indicates full function and $c = 0$ indicates complete failure. This allows Eqs. 11 and 12 to apply at both individual and organizational scales.

Crucially, individuals face inherent risks (failure probability), emerging from the interplay within the network. This is particularly pronounced in athlete groups, where interactions and influence are confined within the sports industry's structure[12,82]. The risk of functional capacity loss (failure) is transient and contingent on the degree of protective investment (p_{p}), determined by each individual's resource pool:

$$p_{\mathrm{p}} = p_{\mathrm{p,max}}/(1 + c_{\mathrm{p},1/2}/(f_{\mathrm{p}}c)) \tag{12}$$

This protection mechanism, encapsulated in Eq. 12, factors in the maximum protection level ($p_{\mathrm{p,max}}$), a reference point ($c_{\mathrm{p},1/2}$), and an evolving protection level ($f_{\mathrm{p}}c$) that integrates individual strategies ($f_{\mathrm{p}0}$ and $f_{\mathrm{p}1}$) and functional capacity (c), updated periodically. Given the constraints in information and decision-making time in sports contexts, individuals resort to heuristic methods to determine their protection level, which lies between a minimum threshold (0.1) and the maximum feasible level (f_{m}):

$$f_{\mathrm{p}} = f_{\mathrm{p}0} + f_{\mathrm{p}1}C \tag{13}$$

This heuristic approach, illustrated in Eq. 13, derives from the eigenvector centrality ($Ax = \lambda x$) of individuals, indicating their influence within the network (C). It encapsulates the micro-scale dynamics of sports systems, where entities (individuals, teams, clubs) navigate risks through imitation and exploration strategies[83,84]. Then, individuals employ a probabilistic imitation mechanism, selecting role models to emulate based on perceived success:

$$p_{\mathrm{i}} = \left[1 + e^{-\omega\,\Delta\pi}\right]^{-1}, \quad \pi_r - \pi_f = \Delta\pi\,|_{\pi_r = role\ model} \tag{14}$$

Here, ω signifies the strength of selection, and $\Delta\pi$ represents the functional capacity disparity between the imitator (π_f) and the role model (π_r). Additionally, individuals are assigned an exploration probability ($p_{\mathrm{e}} \in (0,1)$), allowing them to adjust strategies based on a normal distribution:

$$f\left(x|\mu, \sigma^2\right) = \frac{1}{\sqrt{2\pi\,\sigma^2}} exp^{-\frac{(x-\mu)^2}{2\sigma^2}} \Big| x = individual\ functional\ capacity,\ \ \mu \in R = mean\,(location),\ \ \sigma^2 > 0 = variance\,(squared\ scale) \tag{15}$$

This model, consistent with Eq. 15, suggests that sports systems' members continuously recalibrate their strategies, balancing between established patterns and innovative approaches.

Recovery

In sports systems, the efficacy of immediate interventions for injuries and psychological crises contributes directly to system sustainability through improved treatment outcomes[85] and stakeholder satisfaction[86,87]. Failure in the model originates through a two-stage process. First, each node acquires a failure potential either spontaneously (probability p_{n} per time step) or through propagation from failed neighbors (probability p_{l} per link). Second, this failure potential converts to actual failure with probability $1 - p_{\mathrm{p}}$, where p_{p} is the node's protection

probability defined by Eq. 12. Importantly, p_{p} is individual-specific: it depends on each node's accumulated functional capacity c and protection investment f_{p}, both of which evolve heterogeneously through network-position-dependent imitation and exploration dynamics (Eqs. 13–15; Supplementary Information Sect. 1.2).

To model intervention timing, we introduce a dual-scale recovery mechanism incorporating immediate micro-scale interventions ($r_t \in [0, 1]$) and the broader macro-scale recovery time delay ($t_r \in [0, \infty]$). This approach is modeled as:

$$t_r \in [0, \infty], \; t_r < 1 = \text{strong}, \quad t_r \to \infty = \text{weak} \tag{16}$$

The recovery parameters map to real-world sports interventions: $r_t = 1$ corresponds to immediate intervention (on-field medical attention, instant psychological support), $r_t = 2$: next-day intervention (post-game recovery protocols, day-after debriefing), $r_t > 2$: delayed response system (weekly check-ins, periodic assessments), $r_t > 5$ to critical delay beyond which cascading failures become likely. The parameter r_t is applied uniformly as a system-level policy (e.g., league-wide protocols), while the effective recovery outcome remains individual-specific because nodes with higher $f_{\mathrm{p}} \cdot c$ achieve greater p_{p} upon returning to active state (Eqs. 12–15).

To quantify the combined effect of topology and recovery on system vulnerability, we define the Network Vulnerability Index (NVI):

$$NVI = (N_f \times p_{\mathrm{l}})/(p_{\mathrm{p}} \times (1/r_t)) \tag{17}$$

where N_f represents the mean failure rate, p_{l} is the propagation probability, p_{p} is the average protection probability, and r_t is the recovery time. NVI values above 1.0 indicate critical risk states requiring immediate intervention. This recovery mechanism directly interfaces with the previously outlined operating principles in how risk and failure potentials are mitigated (Supplementary Information Sect. 1.1 and 1.2).

Empirical validation

To ensure that model parameters reflect actual system behaviors[7], we validated predictions against observed failures using three complementary approaches. First, micro-level validation employed comprehensive injury records spanning 13 seasons (n = 77,463 injury events, 30 teams) obtained from publicly available databases (Kaggle, 2023). This dataset captures cascading effects including injury clusters, temporal propagation patterns, and recovery characteristics. Second, macro-level validation used COVID-19 disruption timelines for 12 major professional leagues (NBA, Premier League, La Liga, Serie A, Bundesliga, Ligue 1, MLB, NHL, KBO, K League 1, KBL, NPB) compiled from official league announcements and verified through governing body statements[44]. Third, network size robustness analysis repeated the scale-free network simulation across four sizes (n = 50, 100, 200, 500) with 25 independent realizations per size to confirm that vulnerability patterns are structural properties of the topology rather than artifacts of the specific network scale used in the primary analysis. Detailed data processing procedures, source documentation, and robustness analysis results are provided in Supplementary Information Sect. 4.1–4.2 including the ethics statements.

Statistical analysis

All analyses were conducted using SPSS Statistics (Version 29, IBM), Python 3.8 (Python Software Foundation), and Monte Carlo simulations used 1,000 iterations per network topology. Statistical comparisons employed two-sample t-tests with significance threshold α = 0.05. Model fit was assessed using coefficient of determination (R^2) and root mean square error (RMSE). No corrections for multiple comparisons were applied as each analysis addressed distinct research questions. Sample size (n = 100 nodes) was determined based on computational feasibility while maintaining representative network properties. Code for reproducibility is available at https://github.com/pcw8531/sports-network-risk-propagation.

Ethics declarations

This study used publicly available de-identified NBA injury data from Kaggle (dataset: ghopkins/nba-injuries-2010-2018). COVID-19 sports disruption data were compiled from publicly available official league announcements. Professional athlete network data were obtained from previously published research[12], which received appropriate ethical approval from the original study's institutional review board. No additional ethical approval was required for this secondary analysis of publicly available information.

Data availability

All simulation code and datasets supporting this study are available from a GitHub repository ([https://github.com/pcw8531/sports-network-risk-propagation](https:/github.com/pcw8531/sports-network-risk-propagation)), accessible to peer reviewers and will be made public with a Zenodo DOI upon manuscript acceptance. NBA injury data are publicly available from Kaggle ([https://www.kaggle.com/datasets/ghopkins/nba-injuries-2010-2018](https:/www.kaggle.com/datasets/ghopkins/nba-injuries-2010-2018)). COVID-19 league disruption data were compiled from publicly available official league announcements.

Received: 5 January 2026; Accepted: 23 March 2026
Published online: 27 March 2026

References

1. Leduc, M., Poledna, S. & Thurner, S. Systemic risk management in financial networks with credit default swaps. *arXiv preprint* arXiv:1601.02156 (2017).

2. Pacheco, J. M., Traulsen, A. & Nowak, M. A. Coevolution of strategy and structure in complex networks with dynamical linking. *Phys. Rev. Lett.* **97**, 258103 (2006).
3. Trimmer, P. C. et al. Decision-making under uncertainty: biases and Bayesians. *Anim. Cogn.* **14**, 465–476 (2011).
4. Pastor-Satorras, R., Castellano, C., Van Mieghem, P. & Vespignani, A. Epidemic processes in complex networks. *Rev. Mod. Phys.* **87**, 925 (2015).
5. Choi, S. B., Kang, C. W., Choi, H. J. & Kang, B. Y. Social network analysis for a soccer game. *J. Korean Data Inf. Sci. Soc.* **22**, 1053–1063 (2011).
6. Park, C. W. & Kim, S. Network-Agent systems dynamic modelling: A guide for sport science. *Korean J. Sport Sci.* **31**, 514–533 (2020).
7. Clemente, F. M., Martins, F. M. L. & Mendes, R. S. *Social Network Analysis Applied to Team Sports Analysis* (Springer International Publishing, 2016).
8. Ryan, K., Lu, Z. & Meinertzhagen, I. A. The peripheral nervous system of the ascidian tadpole larva: Types of neurons and their synaptic networks. *J. Comp. Neurol.* **526**, 583–608 (2018).
9. Bock, J. R., Maewal, A. & Gough, D. A. Hitting is contagious in baseball: Evidence from long hitting streaks. *PLoS One* **7**, e51367 (2012).
10. Bunker, R. P. & Thabtah, F. A machine learning framework for sport result prediction. *Appl. Comput. Inform.* **15**, 27–33 (2019).
11. Oldham, M. & Crooks, A. T. Drafting agent-based modeling into basketball analytics. In *2019 Spring Simulation Conference (SpringSim)*, 1–12 (IEEE, 2019).
12. Cui, S. et al. Research on the structure and characteristics of the overall social network of professional athletes. *Complexity* **2021**, 6484098 (2021).
13. Grillner, S. Locomotion in vertebrates: Central mechanisms and reflex interaction. *Physiol. Rev.* **55**, 247–304 (1975).
14. Sussillo, D., Churchland, M. M., Kaufman, M. T. & Shenoy, K. V. A neural network that finds a naturalistic solution for the production of muscle activity. *Nat. Neurosci.* **18**, 1025–1033 (2015).
15. Barsade, S. G. The ripple effect: Emotional contagion and its influence on group behavior. *Adm. Sci. Q.* **47**, 644–675 (2002).
16. Barsade, S. G., Coutifaris, C. G. & Pillemer, J. Emotional contagion in organizational life. *Res. Organ. Behav.* **38**, 137–151 (2018).
17. Bar-Eli, M., Avugos, S. & Raab, M. Twenty years of hot hand research: Review and critique. *Psychol. Sport Exerc.* **7**, 525–553 (2006).
18. Thacker, S. B., Stroup, D. F., Branche, C. M. & Gilchrist, J. Prevention of knee injuries in sports: A systematic review of the literature. *J. Sports Med. Phys. Fitness.* **43**, 165 (2003).
19. Yoon, S. W. & Chung, S. W. Semantic network analysis of legacy news media perception in South Korea: The case of PyeongChang 2018. *Sustainability* **10**, 4027 (2018).
20. Albert, R., Jeong, H. & Barabasi, A. L. Error and attack tolerance of complex networks. *Nature* **406**, 378–382 (2000).
21. Mikaberidze, G., Nag Chowdhury, S., Hastings, A. & D'Souza, R. M. Consensus formation among mobile agents in networks of heterogeneous interaction venues. *Chaos Solitons Fractals* **178**, 114298 (2024).
22. Sjödin, H. et al. COVID-19 healthcare demand and mortality in Sweden in response to non-pharmaceutical mitigation and suppression scenarios. *Int. J. Epidemiol.* **49**, 1443–1453 (2020).
23. Park, C. Potential consequence of interconnected intervention against systemic risk (COVID-19) via a model-driven network-agent dynamic. *Complexity* **2022**, 4805404 (2022).
24. Battiston, S., Gatti, D. D., Gallegati, M., Greenwald, B. & Stiglitz, J. E. Liaisons dangereuses: Increasing connectivity, risk sharing, and systemic risk. *J. Econ. Dyn. Control* **36**, 1121–1141 (2012).
25. Sneppen, K. & Simonsen, L. Impact of superspreaders on dissemination and mitigation of COVID-19. *medRxiv* https://doi.org/10.1101/2020.05.17.20104745 (2020).
26. Park, C. Role of recovery in evolving protection against systemic risk: A mechanical perspective in network-agent dynamics. *Complexity* **2021**, 4805404 (2021).
27. Baron, D. A., Martin, D. M. & Abol Magd, S. Doping in sports and its spread to at-risk populations: An international review. *World Psychiatry* **6**, 118–123 (2007).
28. Lloyd-Smith, J. O., Schreiber, S. J., Kopp, P. E. & Getz, W. M. Superspreading and the effect of individual variation on disease emergence. *Nature* **438**, 355–359 (2005).
29. Ferguson, N. et al. Report 9: Impact of non-pharmaceutical interventions (NPIs) to reduce COVID19 mortality and healthcare demand. *Imperial Coll. Lond.* **10**, 77482 (2020).
30. Böttcher, L., Luković, M., Nagler, J., Havlin, S. & Herrmann, H. J. Failure and recovery in dynamical networks. *Sci. Rep.* **7**, 1–9 (2017).
31. Narizuka, T. & Yamazaki, Y. Characterization of the formation structure in team sports. *arXiv preprint* arXiv:1802.06766 (2018).
32. Romer, L. M., McConnell, A. K. & Jones, D. A. Effects of inspiratory muscle training upon recovery time during high intensity, repetitive sprint activity. *Int. J. Sports Med.* **23**, 353–360 (2002).
33. Mavrommataki, E., Bogdanis, G. C., Kaloupsis, S. & Maridaki, M. Recovery of power output and heart rate kinetics during repeated bouts of rowing exercise with different rest intervals. *J. Sports Sci. Med.* **5**, 115 (2006).
34. Dehmamy, N., Milanlouei, S. & Barabási, A. L. A structural transition in physical networks. *Nature* **563**, 676 (2018).
35. Ribeiro, J., Silva, P., Duarte, R., Davids, K. & Garganta, J. Team sports performance analysed through the lens of social network theory: Implications for research and practice. *Sports Med.* **47**, 1689–1696 (2017).
36. Robins, G., Pattison, P., Kalish, Y. & Lusher, D. An introduction to exponential random graph (p*) models for social networks. *Soc. Netw.* **29**, 173–191 (2007).
37. Kabir, K. A. & Tanimoto, J. Analysis of epidemic outbreaks in two-layer networks with different structures for information spreading and disease diffusion. *Commun. Nonlinear Sci. Numer. Simul.* **72**, 565–574 (2019).
38. Rahmandad, H. & Sterman, J. Heterogeneity and network structure in the dynamics of diffusion: Comparing agent-based and differential equation models. *Manage. Sci.* **54**, 998–1014 (2008).
39. Park, C. Optimizing resilience in sports science through an integrated random network structure: Harnessing the power of failure, payoff, and social dynamics. *Sage Open.* **15**, 21582440251316513 (2025).
40. Smith, A. L. Peer relationships in physical activity contexts: A road less traveled in youth sport and exercise psychology research. *Psychol. Sport Exerc.* **4**, 25–39 (2003).
41. Grund, T. U. Network structure and team performance: The case of English Premier League soccer teams. *Soc. Netw.* **34**, 682–690 (2012).
42. Kugler, P. N. & Turvey, M. T. *Information, Natural Law and the Self-Assembly of Rhythmic Movement* (Erlbaum, 1987).
43. Rosen, R. Some epistemological issues in physics and biology. In *Quantum Implications: Essays in Honor of David Bohm* (eds. Hilley, B. J. & Platt, F. D.) 315–327 (Routledge & Kegan, New York, 1987).
44. World Health Organization. *Coronavirus disease 2019 (COVID-19): Situation report, 72* (World Health Organization, 2020).
45. Barthélémy, M. & Amaral, L. A. N. Small-world networks: Evidence for a crossover picture. *Phys. Rev. Lett.* **82**, 3180 (1999).
46. Lusher, D., Robins, G. & Kremer, P. The application of social network analysis to team sports. *Meas. Phys. Educ. Exerc. Sci.* **14**, 211–224 (2010).
47. Hajihashemi, M. & Samani, K. A. Fixation time in evolutionary graphs: A mean-field approach. *Phys. Rev. E.* **99**, 042304 (2019).
48. Park, C. Network and agent dynamics with evolving protection against systemic risk. *Complexity* **2020**, 1–16 (2020).
49. Kahneman, D. *Thinking, Fast and Slow* (Farrar, Straus and Giroux Macmillan, 2011).
50. Dermine, J. Comment *Swiss J. Econ. Stat.* December, 679–682 (1996).

51. McLaren, C. D. & Spink, K. S. Member communication as network structure: Relationship with task cohesion in sport. *Int. J. Sport Exerc. Psychol.* **18**, 764–778 (2020).
52. Ramos, J., Lopes, R. J. & Araújo, D. What's next in complex networks? Capturing the concept of attacking play in invasive team sports. *Sports Med.* **48**, 17–28 (2018).
53. Grove, J. R., Hanrahan, S. J. & McInman, A. Success/failure bias in attributions across involvement categories in sport. *Pers. Soc. Psychol. Bull.* **17**, 93–97 (1991).
54. McNamara, J. M., Trimmer, P. C. & Houston, A. I. Natural selection can favour "irrational" behaviour. *Biol. Lett.* **10**, 20130935 (2014).
55. Kane, E. J. Principal-agent problems in S&L salvage. *J. Finance* **45**, 755–764 (1990).
56. Gupta, A. & Misra, L. Failure and failure resolution in the US thrift and banking industries. *Financ. Manag.* **28**, 87–105 (1999).
57. Kaufman, G. G. & Seelig, S. A. Post-resolution treatment of depositors at failed banks: Implications for the severity of banking crises, systemic risk, and too-big-to-fail. In *Bank Restructuring and Resolution,* 163–183 (Palgrave Macmillan, London, 2006).
58. Pain, M. A. & Harwood, C. The performance environment of the England youth soccer teams. *J. Sports Sci.* **25**, 1307–1324 (2007).
59. Casey, M. M., Payne, W. R. & Eime, R. M. Organisational readiness and capacity building strategies of sporting organisations to promote health. *Sport Manag. Rev.* **15**, 109–124 (2012).
60. Latash, M. L., Scholz, J. P. & Schöner, G. Toward a new theory of motor synergies. *Motor Control* **11**, 276–308 (2007).
61. Kugler, P. N., Kelso, J. A. S. & Turvey, M. T. On the concept of coordinative structures as dissipative structures: I. theoretical lines of convergence. *Adv. Psychol.* **1**, 3–47 (1980).
62. Bahrke, M. S. Performance-enhancing substance misuse in sport: Risk factors and considerations for success and failure in intervention programs. *Subst. Use Misuse* **47**, 1505–1516 (2012).
63. Vilar, L., Araújo, D., Davids, K. & Bar-Yam, Y. Science of winning soccer: Emergent pattern-forming dynamics in association football. *J. Syst. Sci. Complex.* **26**, 73–84 (2013).
64. Dunning, E. *Sport Matters: Sociological Studies of Sport, Violence, and Civilization* (Routledge, Psychology Press, 1999).
65. Frencken, W., Lemmink, K., Delleman, N. & Visscher, C. Oscillations of centroid position and surface area of soccer teams in small-sided games. *Eur. J. Sport Sci.* **11**, 215–223 (2011).
66. Palacios-Huerta, I. Structural changes during a century of the world's most popular sport. *Stat. Methods Appl.* **13**, 241–258 (2004).
67. Saavedra, S., Powers, S., McCotter, T., Porter, M. A. & Mucha, P. J. Mutually-antagonistic interactions in baseball networks. *Phys. A*. **389**, 1131–1141 (2010).
68. Kivelä, M. et al. Multilayer networks. *J. Complex Netw.* **2**, 203–271 (2014).
69. Mucha, P. J., Richardson, T., Macon, K., Porter, M. A. & Onnela, J. P. Community structure in time-dependent, multiscale, and multiplex networks. *Science* **328**, 876–878 (2010).
70. Helbing, D. Globally networked risks and how to respond. *Nature* **497**, 51 (2013).
71. Rebar, A. L. Automatic regulation used in sport and exercise research. In *Oxford Research Encyclopedia of Psychology* (Oxford University Press, 2017).
72. Vespignani, A. Twenty years of network science. *Nature* **558**, 528–529 (2018).
73. Hoang, H. & Antoncic, B. Network-based research in entrepreneurship: A critical review. *J. Bus. Venturing* **18**, 165–187 (2003).
74. Fortunato, S. Community detection in graphs. *Phys. Rep.* **486**, 75–174 (2010).
75. Purves, D. et al. *Neuroscience* 2nd edn. (Sinauer, 2001).
76. Cowan, R. & Jonard, N. Network structure and the diffusion of knowledge. *J. Econ. Dyn. Control.* **28**, 1557–1575 (2004).
77. Huang, Q. et al. Modeling for professional athletes' social networks based on statistical machine learning. *IEEE Access* **8**, 4301–4310 (2019).
78. Erdős, P. & Rényi, A. On Cantor's series with convergent ∑1/qn. *Ann. Univ. Sci. Budapest De Rol Eötvös Nom* **II**, 93–109 (1959).
79. Watts, D. J. & Strogatz, S. H. Collective dynamics of "small-world" networks. *Nature* **393**, 440–442 (1998).
80. Barabási, A. L. & Albert, R. Emergence of scaling in random networks. *Science* **286**, 509–512 (1999).
81. Rosen, S. & Sanderson, A. Labour markets in professional sports. *Econ. J.* **111**, F47–F68 (2001).
82. Zhao, N. Athlete social support network modeling based on modern valence bond theory. *Complexity* **2020**, 4392975 (2020).
83. Hadders-Algra, M. Early human motor development: From variation to the ability to vary and adapt. *Neurosci. Biobehav. Rev.* **90**, 411–427 (2018).
84. Sharapov, D. & Ross, J. M. Whom should a leader imitate? Using rivalry-based imitation to manage strategic risk in changing environments. *Strateg. Manag. J.* https://doi.org/10.1002/smj.3120 (2019).
85. Moser, R. S., Glatts, C. & Schatz, P. Efficacy of immediate and delayed cognitive and physical rest for treatment of sports-related concussion. *J. Pediatr.* **161**, 922–926 (2012).
86. Murphy, S. M. *Sport Psychology Interventions* (Human Kinetics, 1995).
87. Holmes, P. S. & Wright, D. J. Motor cognition and neuroscience in sport psychology. *Curr. Opin. Psychol.* **16**, 43–47 (2017).

Author contributions

C.P. conceived and designed the study, developed the network-agent model, performed simulations, analyzed the data, conducted empirical validation, and wrote the manuscript.

Funding

This work was supported by the Basic Science Research Program through the National Research Foundation of Korea (NRF), funded by the Ministry of Education (grant no. 2020R1I1A1A01056967). This work was also supported by Seoul National University BK21 Four Program.

Declarations

Competing interests

The authors declare no competing interests.

Additional information

Supplementary Information The online version contains supplementary material available at https://doi.org/10.1038/s41598-026-45805-6.

Correspondence and requests for materials should be addressed to C.P.

Reprints and permissions information is available at www.nature.com/reprints.